Paper

Effect of aluminum source on flexural strength of mullite-bonded porous silicon carbide ceramics

B. V. Manoj KUMAR, Jung-Hye EOM, Young-Wook KIM,[†] In-Sub HAN[*] and Sang-Kuk WOO[*]

Department of Materials Science and Engineering, the University of Seoul, 90, Jeonnong-dong, Dongdaemun-gu, Seoul 130−743, Korea
[*]Energy Materials Research Center, Korea Institute of Energy Research, 71−2, Jang-dong, Yuseong-gu, Daejeon 305−343, Korea

In the present work, four aluminum sources (Al/AlN/Al$_2$O$_3$/Al(OH)$_3$) were used to fabricate mullite-bonded porous SiC ceramics via reaction sintering in air at 1450°C and 1550°C for 1–6 h duration, and the role of aluminum source on microstructure and strength was estimated. The microstructures revealed a variation in necking and adhesion characteristics of SiC/mullite/silica grains. The porosity decreased and strength increased with sintering temperature or time for all specimens, except for the one prepared with Al$_2$O$_3$. Amongst the investigated, SiC ceramics prepared with Al$_2$O$_3$ exhibited the lowest porosity of 17% and highest specific strength of 19 kN.m/kg, while the usage of AlN rendered a combination of the highest porosity of 42% and lowest specific strength of 5 kN.m/kg. An attempt has been made to qualitatively explain the strength variation of prepared ceramics on the basis of contributing oxidation reactions towards mullitization.

1. Introduction

Porous SiC ceramics with a unique combination of good mechanical properties, thermal- shock resistance and chemical stability are considered to be candidate materials for several applications such as hot gas filters, molten metal filters, diesel particulate filters, catalytic supports, membrane supports for hydrogen separation, gas-burner media, and preforms for production of metal matrix composites.[1)–4)] Porous SiC ceramics can be produced mainly by replica, sacrificial template, and reaction sintering methods.[5)–7)] Considering the good oxidation resistance and high temperature stability, and small difference in thermal expansion coefficients with SiC (0.6×10^{-6}/K at 273–1273 K), mullite-SiC composites are expected to exhibit better properties.[8)–14)] It has been reported that oxidation-derived SiO$_2$ and alumina react in situ to fabricate mullite (3Al$_2$O$_3$. 2SiO$_2$)-bonded porous SiC ceramics at 1400–1550°C in air.[15)–17)] During sintering of SiC, Al$_2$O$_3$ and graphite powder compacts, graphite is burned out to produce pores and the surface of the SiC is oxidized to SiO$_2$ at high temperature. Upon increasing the temperature, SiO$_2$ reacts with Al$_2$O$_3$ to form mullite.[15)] A maximum of strength of 28 MPa was obtained with 20 μm- starting SiC powder and Y$_2$O$_3$ sintering additives.[16)] Eom et al. demonstrated that strength can be increased to 39 MPa for a 37% porous mullite-bonded SiC ceramics when high alumina content (37 mass%) was used, without using graphite.[18)] The same group further reported that strength can be improved to ~ 90 MPa using sub-micron SiC powders.[19)] In order to explore the potential, a thorough understanding of the influence of processing chemistry on mechanical properties of these important materials is highly required. It is clear from the literature review[11)–19)] that in situ participation of alumina towards mullitization is significant in improving the strength of the porous ceramics. However, no study has been reported towards estimating the contribution of alumina from

various sources on the microstructure and mechanical properties of porous mullite-bonded SiC ceramics.

In the above connection, four aluminum sources: aluminum, aluminum nitride, alumina and aluminum hydroxide powders were used in the present work to in situ synthesize mullite phase with SiC powders via reaction sintering in air and the influence of aluminum source on synthesis of mullite phase, relative density, and flexural strength of porous SiC ceramics is systematically studied. Coarse (~65 μm) SiC powders were used in the present study to keep the processing cost low.

2. Experimental procedure

Commercially available refractory-grade SiC (~65 μm, Showa Denko K. K.), sub-micron SiC powders (~0.5 μm, Norton AS, Norway), Al (3 μm, 99.9% pure, High Purity Chemicals Osaka), AlN (1.3 μm, Grade F, Tokuyama Soda Co.), Al$_2$O$_3$ (~0.4 μm, AKP30, Sumitomo Chemical Co.) and Al(OH)$_3$ (~2 μm, Kanto Chemical Co., Inc.) were used as starting materials. Four batches of powder mixtures were prepared with the respective aluminum source content (see **Table 1**). The initial calculated aluminum content (23. 7 mass%) in each source as well as the ratio of large SiC content to sub-micron SiC content (2.3:1) were same. All batches were milled separately in polypropylene jar for 24 h

Table 1. Details of Batch Composition, Green Density and Green Porosity of the Investigated Powder Mixtures

| Sample | Batch composition (mass%) | | | | | | Green density (g/cm³) | Green porosity (%) |
	SiC (~65 μm)	SiC (~0.5 μm)	Al	AlN	Al$_2$O$_3$	Al (OH)$_3$		
MBSC1	53.4	22.9	23.7				1.82	40.9
MBSC2	47.5	20.4		32.1			1.73	45.4
MBSC3	44.1	18.9			37.0		2.22	35.9
MBSC4	36.9	15.8				47.3	1.94	34.8

[†] Corresponding author: Y.-W. Kim; E-mail: ywkim@uos.ac.kr

using distilled water and SiC grinding balls. Polyethylene glycol and polyvinyl alcohol were added as binders. The milled slurry was dried at 100°C for 24 h and uniaxially pressed under a pressure of 50 MPa using 35 mm × 8 mm mold. The compacts were sintered at 1450°C and 1500°C for 1 h, 2 h and 6 h in air. The density of the green compacts and the bulk density of the sintered ceramics were calculated from the weight-to-volume ratio. The porosity was estimated using boiling water. The fracture surface morphology was studied using scanning electron microscopy (SEM, S4300, Hitachi Ltd.). Bar-shaped samples were cut to a size of 3 mm × 4 mm × 30 mm and bending tests were performed at room temperature on four to five specimens at each condition using a four-point method (Instron 4465, Instron Co., Ltd., USA) with inner and outer spans of 10 and 20 mm, respectively. The specimens were loaded at a constant crosshead speed of 0.5 mm/min. All surfaces of the sintered samples were polished and subsequently samples were ground using mortar. The powder was sieved (through $600\,\mu$m) and the phase analysis conducted using X-ray diffractometry (XRD, D8 Discover, Bruker AXS GmbH, Germany) with Cu Kα radiation. Differential thermal analysis (DTA) of powder mixtures of varying composition was carried up to 1500°C in air with 4°C/min heating/cooling rate using SDT Q600 V7.0 Build 84 (Universal v4.0C TA Instruments) system.

3. Results

The effect of aluminum source on phase evolution of the sintered ceramics is shown in **Fig. 1**(a). A 70 mass% SiC- 30 mass% mullite composite powder mixture synthesized at 1600°C for 2 h was used to analyze various phases present in the sintered mullite-bonded porous SiC ceramics. XRD analysis reveal major peaks of α-SiC, mullite, cristobalite, and traces of α-Al$_2$O$_3$. With increase in temperature from 1450°C to 1550°C, alumina peaks were reduced in intensity. With the traces of alumina peaks, the mullitization reaction is nearly completed when sintered at 1550°C. However, the phase evolution varied with different aluminum sources used. For the purpose of comparative estimation of the degree of mullitization, the mullite phase content was assessed from the fraction of major peak intensities that appear on the XRD spectrum of the samples sintered at 1550°C for 6 h, and presented in Fig. 1(b). It is evident that MBSC3 possess the highest amount (26%) of mullite, while MBSC2 has the lowest mullite (17%). The MBSC1 and MBSC4 have mullite in between.

The green density measurements of the investigated powder mixtures are shown in Table 1. It is evident that the green density of the MBSC3 is the highest and that of MBSC2 is the lowest among the investigated ceramics. The green density of the MBSC1 and MBSC4 are in between. The fine Al$_2$O$_3$ powder rendered a maximum green density. However, there is no relation between particle size and green density for other specimens. This is probably related to the other characteristics of powder particles such as size distribution and shape. Furthermore, it is evident from Table 1 and Fig. 1(b) that the green porosity and degree of mullitization are generally related. The large degree of particle contacts with the low green porosities in MBSC3 or MBSC4 results in the promoted reaction to yield high mullite content. According to Carter,[20] the completeness (kinetics) of solid state diffusion reaction at high temperature to produce a volume of reaction product from a unit volume of reactant is governed by the reactant particle size. Fine particles largely promote the reaction because of the decreased diffusion distances. On the other hand, the growth of the solid state reaction product in powder systems essentially occurs at particle contact points. Thus, combined effect of reactant particle size (due to different aluminum sources) and degree of green body particle contacts (variation in green porosity) in the present study influences the degree of mullitization. Results indicate that fine particle size and low green porosity yield greater mullitization.

Figure 2 shows typical fracture surfaces of porous mullite-bonded SiC ceramics using different sources of aluminum. In general, microstructures of the samples sintered at 1550°C for 2 h reveal large SiC grains embedded in matrix of fine and loosely bound grains and residual porosity. Since mullitization occurs before densification, the latter is limited to a smaller extent, resulting in structure containing plenty of open pores.[21] The pores are derived from stacking of SiC and Al/AlN/Al$_2$O$_3$/Al(OH)$_3$ particles. The grain size of mullite or silica ranges from 0.5 to $2\,\mu$m, while pore size ranges from 1 to $5\,\mu$m. It is difficult to distinguish the grains in these microstructures. Amongst the investigated ceramics, MBSC3 exhibits strongest microstructure of well connected small mullite/silica particles that attached with large SiC grains (Fig. 2(c)). The shrinkage is also the higher for this sample, rendering the lowest porosity. On the other hand, MBSC1 consists of very loosely bound particles with minimal necking, suggesting less strength (Fig. 2(a)). In case of MBSC2, less shrinkage results in increased porosity (Fig. 2(b)). The
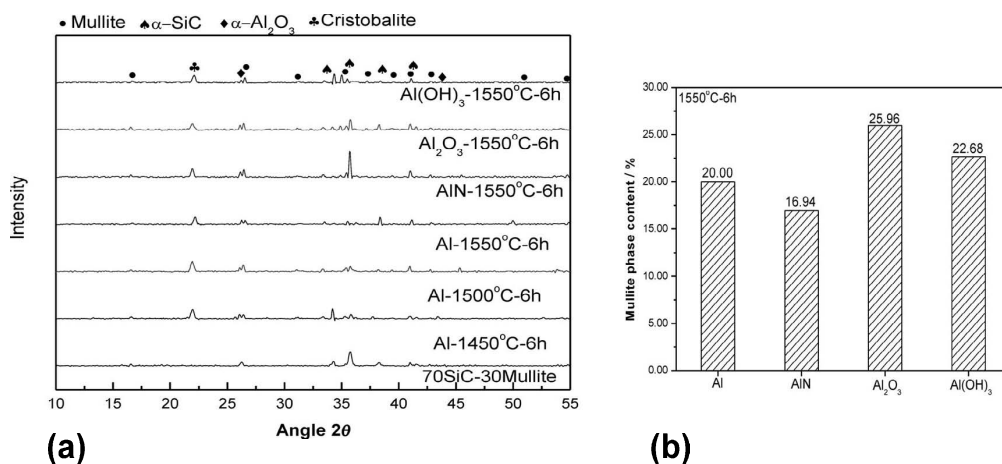

Fig. 1.   (a) Phase analysis of the porous mullite-bonded SiC ceramics and (b) mullite phase content of the ceramics sintered at 1550°C for 6 h.
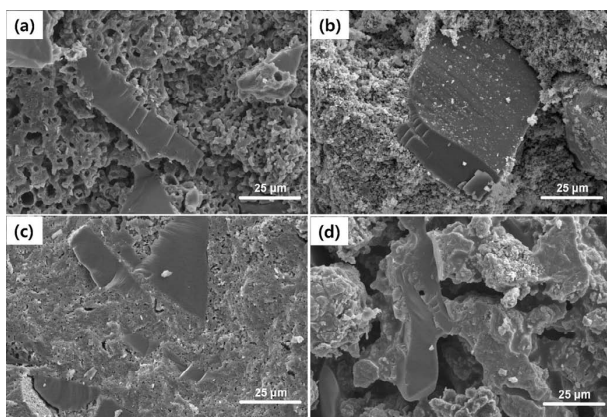
Fig. 2. Typical fracture surfaces of the porous mullite-bonded SiC ceramics sintered at 1550°C for 2 h in air with various aluminum sources: (a) Al, (b) AlN, (c) Al_2O_3 and (c) $Al(OH)_3$.
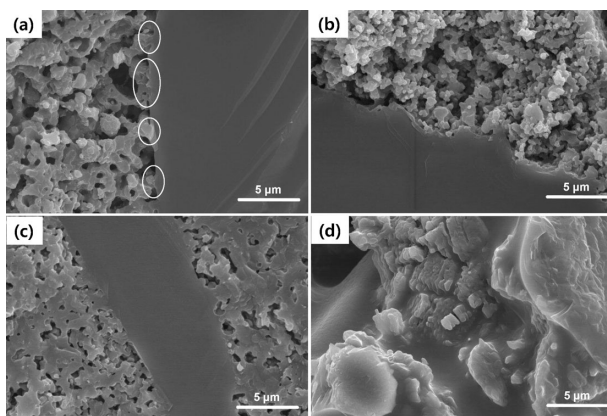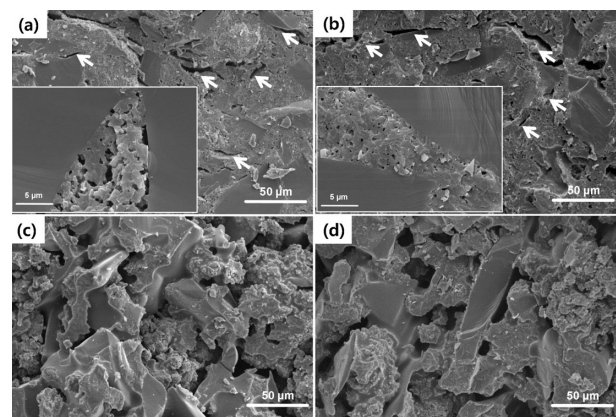

Fig. 4. Typical fracture surfaces of the MBSC3 specimen sintered for (a) 1 h (b) 6 h, and MBSC4 specimen sintered for (c) 1 h and (d) 6 h in air at 1550°C. Insets in (a) and (b) show the bonding characteristics. Arrows indicate extensive cracking.

Fig. 3. Bonding characteristics of the porous mullite-bonded SiC ceramics sintered at 1550°C for 2 h in air with various aluminum source: (a) Al, (b) AlN, (c) Al_2O_3 and (c) $Al(OH)_3$. Ellipse marks indicate discontinuous bonding.

microstructure of MBSC4 seems to be different (Fig. 2(d)). The small particles are strongly necked but weakly attached with large SiC grains. Moreover, pore size is tremendously increased. Another important observation is that the large grains are fractured predominantly by transgranular mode in MBSC3, MBSC1 or MBSC4 sample, while pull-out of large SiC grain indicates intergranular fracture in MBSC2.

The influence of aluminum source on the bonding characteristics of grain interface of ceramics sintered at 1550°C for 2 h is further explored in **Fig. 3**. The discontinuous bonding (marked with ellipses in Fig. 3(a)) of small mullite/silica grains with large SiC grains can be found in MBSC1, while intimate adhesion of well connected small grains with large SiC grains can be observed in MBSC3. On the other hand, the small particles with weak necking are poorly attached with the large SiC grains in MBSC2 (Fig. 3(b)). In case of MBSC4, the particles are strongly connected but weakly attached with large SiC grains, resulting in an increased pore size (Fig. 3(d)). The strongest adhesion of highly necked particles with large SiC grains is expected to impart high strength in case of MBSC3 (Fig. 3(c)).

The influence of sintering duration on microstructural characteristics is shown in **Fig. 4**. The prolonged sintering results in densification at local regions, attributed to the more amount of

mullite phase. The increased adhesion between small grains and large SiC grains with prolonged sintering duration can be noted in insets of Figs. 4(a) and (b). However, the evidence of enhanced cracking (marked with arrows in Figs. 4(a) and (b)) with sintering duration of MBSC3 might circumvent the strength improvement by certain extent. In MBSC4 sample, the increased duration enhanced the necking of small particles but large pore size is still observed, without obvious attachment of large SiC grains (Figs. 4(c) and (d)).

The porosity measurements are shown in **Fig. 5**. The porosity varied from 17–42% with the variation in the aluminum source and sintering conditions. When sintered at 1450°C, MBSC3 render minimum porosity, while MBSC4 provides maximum amongst the investigated specimens. The increase in sintering temperature reduced porosity by 1–7%, whereas duration caused reduction by 1–5%. Thus, a minimum porosity of ~17% was recorded for MBSC3 sintered for 6 h, whereas a maximum porosity of 42% was measured for MBSC2 sintered for 1 h duration at 1450°C. When sintered at 1550°C, MBSC2 exhibited a maximum porosity of 40% after 1 h and MBSC3 rendered a minimum porosity of 17% after 6 h. Overall, MBSC3 has a minimum amount of porosity and MBSC2 has maximum, and MBSC1 and MBSC4 have porosities in between, irrespective of the sintering conditions.

In order to avoid the shrinkage effect in understanding the influence of aluminum source, the variation of specific flexural strength of the mullite-bonded SiC composites sintered at different sintering conditions is shown in **Fig. 6**. It is evident that specific strength varied in a range of 5–19 kN.m/kg for the developed ceramics. Among the investigated specimens, MBSC2 exhibited poor strength of 5 kN.m/kg, while MBSC3 exhibited a high strength level of 19 kN.m/kg when sintered at 1450°C for 1 h. When sintered at high temperature, the specific strength increased by 1–5 kN.m/kg for all specimens, except MBSC3. A reduction of 4–5 kN.m/kg was observed for MBSC3 with increase in temperature from 1450°C to 1550°C. With increase in duration, the specific strength in general increased.

The variation in strength can be related to the observed microstructural characteristics of the sintered specimens. MBSC3 microstructure with strong network of mullite/silica grains that strongly adhere with large SiC grains imparts highest strength. MBSC1 microstructure with weakly connected grains and dis-
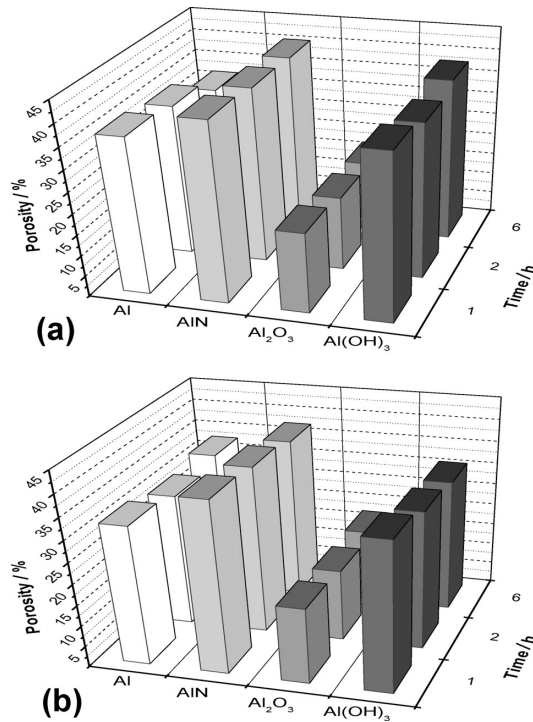
(a)

(b)

Fig. 5. Effects of Al source and sintering time on porosity of porous mullite-bonded SiC ceramics: (a) 1450°C and (b) 1550°C.

(a)

(b)

Fig. 6. Effects of Al source and sintering time on specific strength of porous mullite-bonded SiC ceramics: (a) 1450°C and (b) 1550°C.

continuous adhesion result in the low strength than MBSC3. MBSC4 sample consisting of strong necking of small grains with weak adhesion to the large SiC grains provide large porosity. The increased defect (pore) size helps to easy crack propagation that renders less strength. The very loose structure of mullite/silica grains and their poor adhesion with large SiC grains offers lowest strength in case of MBSC2. The intergranular fracture observed in MBSC2 also indicates its poor strength when compared with transgranular fracture in other samples.

4. Discussion

As the sinterability or strength of the sintered specimens is claimed to be largely affected by the packing density of the green body,[22)–24)] the influence of aluminum source on the relationship between green density and porosity, density or strength of the sintered specimens in the present study can be discussed. In general, compacts of low green density resulted in high sintered porosity, regardless of the sintering temperature and duration. Typical relation between green density and sintered porosity of the specimens sintered at 1550°C for 6 h is provided in **Fig. 7**(a). MBSC2 specimen prepared with the compacts of lowest green density of 1.73 g/cm^3 consisted of a maximum porosity of ~37%, while MBSC3 specimen prepared with compacts of highest green density of 2.22 g/cm^3 exhibited a minimum porosity of ~17%. However, the corresponding relationship between the green density and sintered density of the specimen is not observed (Fig. 7(b)). Particularly, 1.94 g/cm^3 green density resulted in a low sintered density of 1.85 g/cm^3 in case of MBSC4, when compared against 1.82 g/cm^3 green density and 1.86 g/cm^3 sintered density for MBSC1. This deviation in case of MBSC4 is also observed in relationship between green porosity and sintered porosity (Fig. 7(c)). The weight loss due to decomposition of Al(OH)$_3$ during sintering is probably responsible for the observed low density for MBSC4. Furthermore, MBSC1
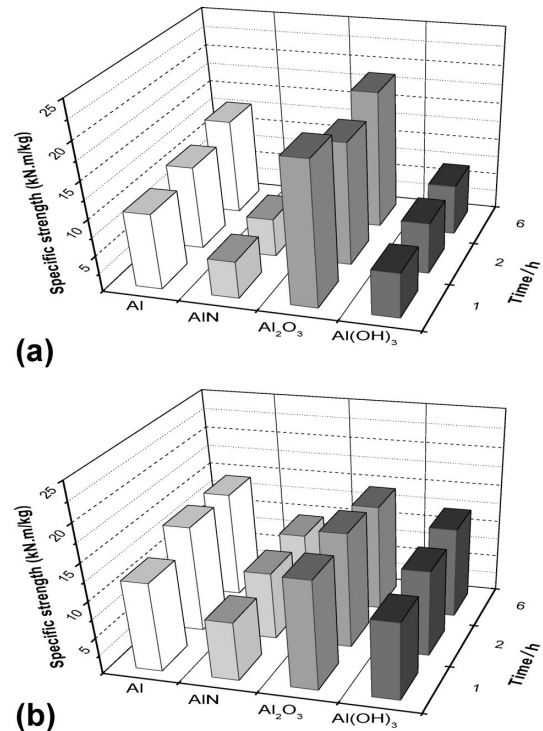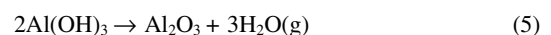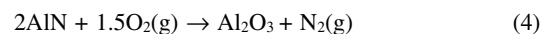
specimen prepared with the green density of 1.82 g/cm^3 showed high strength of ~27 MPa when compared against ~23 MPa strength and 1.94 g/cm^3 density for MBSC4 (Fig. 7(d)). The observed high strength for MBSC1 can be attributed to the greater feasibility of alumina formation. These results necessarily suggest that porosity is largely determined by the green density regardless of the aluminum source, while composition of the staring powder mixture (aluminum source) also influences the density or strength of the sintered SiC ceramics via variety of sintering reactions.

The formation of mullite phase in between SiC grains can be explained on the basis of in situ reactions. SiC oxidizes to amorphous silica that further crystallizes to form cristobalite during sintering at high temperatures in air[25)] as

$$SiC + 2O_2 \rightarrow SiO_2 \text{ (amorphous)} + CO_2(g) \quad (1)$$

$$\text{Amorphous } SiO_2 \rightarrow \text{Cristobalite} \quad (2)$$

Simultaneously, the alumina is formed from various sources as per the following oxidation reactions:

$$2Al + 1.5O_2(g) \rightarrow Al_2O_3 \quad (3)$$

$$2AlN + 1.5O_2(g) \rightarrow Al_2O_3 + N_2(g) \quad (4)$$

$$2Al(OH)_3 \rightarrow Al_2O_3 + 3H_2O(g) \quad (5)$$

The cristobalite reacts with alumina/derived-alumina upon increasing the temperature (beyond 1400°C) to form mullite according to:[8),15)]

$$3Al_2O_3 + 2SiO_2 \rightarrow 3Al_2O_3.2 SiO_2 \text{ (mullite)} \quad (6)$$
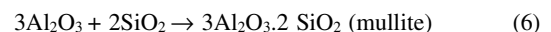
The mullitization is followed by the partial liquid phase sintering that is responsible for densification. The in situ synthesized mullite acts as an adhesive, bonding the SiC particles together, as observed in Figs. 2–4. **Figure 8** represents DTA
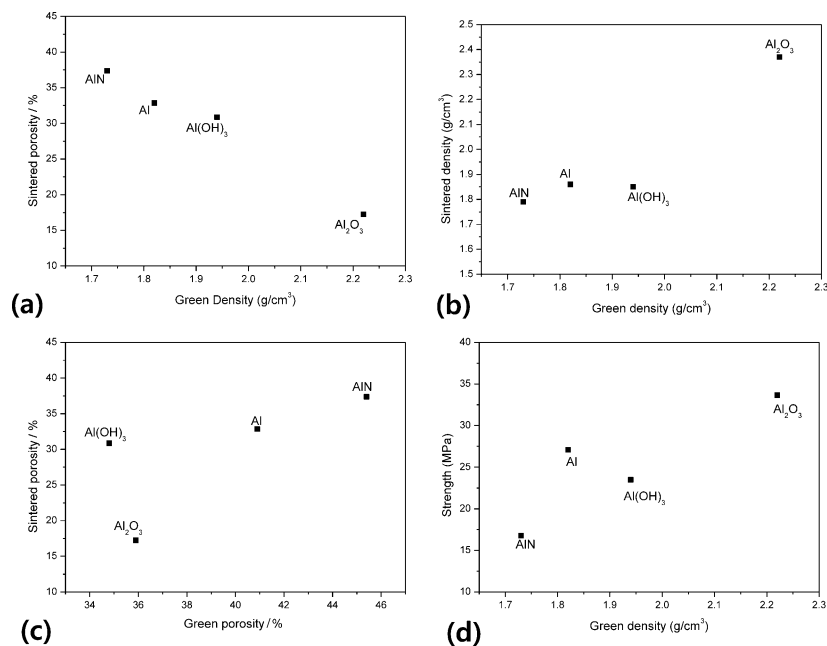
Fig. 7. The relationship between (a) green density and sintered porosity, (b) green density and sintered density, (c) green porosity and sintered porosity, and (d) green density and strength of the specimens sintered at 1550°C for 6 h.
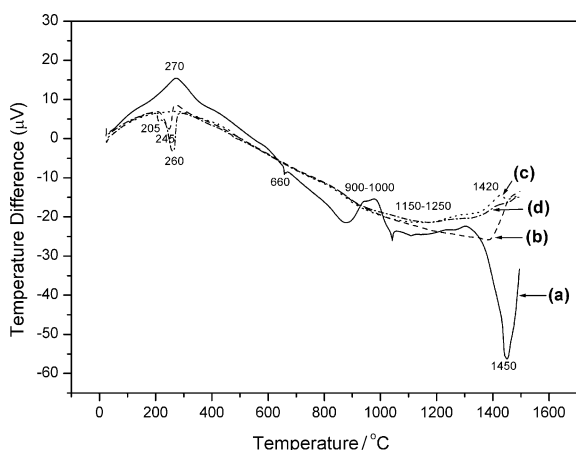

Fig. 8. DTA curves of the powder mixtures containing various aluminum sources: (a) Al, (b) AlN, (c) Al_2O_3 and (d) $Al(OH)_3$.

curves of the investigated powder mixtures that differ in aluminum sources: Al, AlN, Al_2O_3 and $Al(OH)_3$. Endothermic peaks at 205°C (curve (d)) and 245°C (curve (b)) represent respective decomposition reactions of $Al(OH)_3$ and AlN (Eq. 4), while large endothermic peak at 260°C (curve (d)) indicates the dehydration reaction of $Al(OH)_3$ (Eq. 5). The appearance of sharp exothermic peak at 270°C (curve (a)) represents rapid solid state oxidation of Al particles (Eq. 3) whereas shallow peak at around 245°C (curve (c)) reveals greater stability of Al_2O_3 particles. The endothermic peak at 660°C (curve (a)) essentially indicates the melting of Al. Upon further heating, the presence of shallow exothermic peak in the temperature range of 900–1000°C (curve (a)) indicates the oxidation of molten Al. This can be thought also as a result of the oxidation of inner part of the particles that was protected by the oxide layer that formed due to initial solid state oxidation at 270°C. The shallow peak in the range of 1150–1250°C in all curves indicate the oxidation of SiC particles (Eq. 1). Oxidation of SiC at lower temperature (usually occurs beyond

1350°C)[26] is due to the increased reaction kinetics caused by the large surface area of submicron particles. The exothermic peak at 1420°C (curve (c)) represents the mullitization reaction (Eq. 6) when Al_2O_3 particles were used. The observed temperature is consistent with the reported mullite reaction temperature range of 1400–1450°C.[15),27)] However such a distinguishable peak does not exist in the DTA curves of other powder mixtures upto the maximum temperature studied (1500°C). The increase in the slopes of the curves indicate the onset of mullitization (Eq. 6) however, absence of distinguishable peak within the 1500°C represents the incompleteness. The onset of the mullite reaction is estimated as 1370°C (curve (d)), 1390°C (curve (b)) and beyond 1500°C (curve (a)) for the respective powder mixtures containing $Al(OH)_3$, AlN and Al. The presence of sharp endothermic peak at 1450°C for Al is not understood. Overall, it is evident that the reaction temperatures are significantly different with the compositional variation of powder mixtures thus influencing the microstructure and mechanical properties of mullite-bonded SiC ceramics.

Furthermore, XRD analysis (not shown) of the submicron SiC particles heated upto 1550°C for 6 h in air revealed the predominant presence of cristobalite and a small amount (~15%) of retained SiC phase. Since the amount of submicron SiC particles in the initial powder mixtures is same in the present study, the role of their oxidation in influencing the degree of mullitization is expected be insignificant. Thus, small grains in Figs. 2–4 are mainly mullite/silica/SiC that attached with the large SiC grains. The mullitization between SiO_2 and Al_2O_3 can be explained by the solution-precipitation mechanism.[28),29)] Due to the superficial softening, the Al_2O_3 particles penetrate into the viscous SiO_2 glass, leading to the nucleation of mullite. At increased temperature, viscosity of SiO_2 glass decreases and more Al^{3+} ions are dissolved into the SiO_2 glass. The mullite formation is accelerated because of the short diffusion distances and is diffusion controlled.[16)] Accordingly, strength improved in general with temperature or time except for MBSC3. While, readily available alumina is consumed to a larger extent in MBSC3, the SiC-rich composition cause deficiency in alumina for further mullitization

resulting in the excessive amount of residual cristobalite SiO_2. The phase transformation of cristobalite from tetragonal to cubic induces cracks (see Fig. 4) in sintered specimen during cooling. Moreover, the excessive amount of cristobalite is harmful to high temperature properties of porous SiC ceramics because of its large coefficient of thermal expansion (17.5×10^{-6}/K at $20 - 700°C$).[16] Thus, strength is reduced with increase in temperature or time for MBSC3. The poor strength of MBSC2 sample can be understood from the oxidation of AlN. The oxidation of AlN to Al_2O_3 is highly favored above 1100°C in oxidizing atmospheres as per Eq. 4.[30] It is to note that the oxidation of AlN is largely affected by the simultaneous oxidation of SiC from the SiC-rich composition in the present study. It has been reported that high temperature oxidation of the AlN can be effectively suppressed in the presence of silica.[31] Accordingly, silica derived from SiC particles in the present system also protects AlN particles from oxidation due to the inhibition of transport of oxidants (O_2). Thus, limited amount of alumina is available for the mullitization to occur and responsible for the lowest strength levels observed in case of MBSC2 (Fig. 6).

Summarizing, porosity of mullite-bonded porous SiC ceramics could be related to the green density of powder mixture, while influence of aluminum source was significant in assessing the sintered density, mullitization or strength. The high degree of mullitization from the readily available alumina in MBSC3 resulted in the highest strength values, whereas oxidation-derived alumina in MBSC1 rendered relatively low strength. The suppressed oxidation of AlN in presence of silica effectively reduced the mullitization and thereby strength to the lowest levels for MBSC2. The strength increased with sintering temperature and duration due to the accelerated diffusion of oxygen through silica for MBSC1, MBSC2 and MBSC4, while the excessive amount of residual cristobalite was attributed to the reduced strength in case of MBSC3. In the backdrop of above considerations and based on the experimental results obtained, it can be mentioned that the AlN shall not be used for fabricating stronger porous mullite-bonded SiC ceramics via reaction sintering.

5. Conclusions

Mullite-bonded porous SiC ceramics were fabricated using different aluminum sources: Al, AlN, Al_2O_3 and $Al(OH)_3$ via reaction sintering in air at 1450°C and 1550°C for 1 h, 2 h and 6 h duration. The role of aluminum source on the mullitization, microstructural development and strength was assessed. The following are the major conclusions:

(a) The mullitization increased with sintering temperature and almost completed when sintered at 1550°C. The sintering duration increased the mullitization for all specimens.

(b) The microstructures in general consisted of loose grain structure with obvious pores. The mullite-silica grains were well connected and strongly adhered with large SiC grains in samples fabricated using Al_2O_3 source, whereas samples prepared with AlN source showed poor adhesion and weak bonding.

(c) A minimum porosity of 17% was measured for the sample prepared with Al_2O_3 source when sintered at 1550°C for 6 h, while a maximum porosity of 42% measured for the samples prepared with AlN source when sintered at 1450°C for 1 h.

(d) High specific strength levels of 14–19 kN.m/kg were measured for samples fabricated using Al_2O_3 source, while samples prepared with AlN source rendered poor strength levels of 5–9 kN.m/kg with varying sintering conditions.

(e) The variation in the strength can be largely explained on the basis of contribution of sintering reactions towards mullitization.

References

1) D. J. Green and P. Colombo, *MRS Bull.*, **28**, 296–300 (2003).
2) P. Greil, *Adv. Mater.*, **14**, 709–716 (2002).
3) S. Kitaoka, Y. Matsushima, C. Chen and H. Awaji, *J. Am. Ceram. Soc.*, **87**, 906–913 (2004).
4) X. Zhu, D. Jiang and S. Tan, *Mater. Sci. Eng. A*, **323**, 232–238 (2002).
5) J.-H. Eom, Y.-W. Kim, I. H. Song and H. D. Kim, *J. Eur. Ceram. Soc.*, **28**, 1029–1035 (2008).
6) J. F. Yang, G. J. Zhang, N. Kondo, J. H. She, Z. H. Jin, T. Ohji and S. Kanzaki, *J. Am. Ceram. Soc.*, **86**, 910–914 (2003).
7) Y.-W. Kim, S. H. Kim, I. H. Song, H. D. Kim and C. B. Park, *J. Am. Ceram. Soc.*, **88**, 2949–2951 (2005).
8) I. A. Aksay, D. M. Dabbs and M. Sarikaya, *J. Am. Ceram. Soc.*, **74**, 2343–2358 (1991).
9) H. R. Rezaie, W. M. Rainforth and W. E. Lee, *J. Eur. Ceram. Soc.*, **19**, 1777–1787 (1999).
10) M. I. Osendi, *J. Mater. Sci.*, **25**, 3561–3565 (1990).
11) B. Saruhan, W. Albers, H. Schneider and W. A. Kaysser, *J. Eur. Ceram. Soc.*, **16**, 1075–1081 (1996).
12) A. P. S. Rana, O. Aiko and J. A. Pask, *Ceram. Int.*, **8**, 151–153 (1982).
13) Y. Hirata, S. Matsushita, Y. Ishihara and H. Katsuki, *J. Am. Ceram. Soc.*, **74**, 2438–2442 (1991).
14) M. Schmticker, W. Albers and H. Schneider, *J. Eur. Ceram. Soc.*, **14**, 511–515 (1994).
15) S. Ding, S. Zhu, Y. Zeng and D. Jiang, *Ceram. Int.*, **32**, 461–466 (2006).
16) S. Ding, S. Zhu, Y. Zeng and D. Jiang, *J. Eur. Ceram. Soc.*, **27**, 2095–2102 (2007).
17) S. Ding, Y. P. Zen and D. Jiang, *J. Phys. D: Appl. Phys.*, **40**, 2138–2142 (2007).
18) J.-H. Eom, Y.-W. Kim and S.-K. Woo, *J. Ceram. Proc. Res.*, **10**, s82–s86 (2009).
19) J.-H. Eom, Y.-W. Kim, S.-K. Woo and I.-S. Han, *J. Ceram Soc. Japan*, **117**, 421–425 (2009).
20) (a) R. E. Carter, *J. Chem. Phys.*, **34**, 2010–2015 (1961).
    (b) R. E. Carter, *J. Chem. Phys.*, **35**, 1137–1138 (1961).
21) Y. Nurishi and J. A. Pask, *Ceram. Int.*, **8**, 57–59 (1982).
22) H. Takahashi, N. Shinohara, K. Uematsu and J. Tsubaki, *J. Am. Ceram. Soc.*, **79**, 843–848 (1996).
23) Y. Zhang, M. Inoue, N. Uchida and K. Uematsu, *J. Mater. Res.*, **14**, 3370–3374 (1999).
24) N. Shinohara, S. Katori, M. Okumiya, T. Hotta, K. Nakahira, M. Naito, Y.-I. Cho and K. Uematsu, *J. Eur. Ceram. Soc.*, **22**, 2841–2848 (2002).
25) P. J. Jorgensen, M. E. Wadsworth and I. B. Cutler, *J. Am. Ceram. Soc.*, **42**, 613–616 (1959).
26) V. A. Lavrenko, E. A. Pugach, S. I. Filipchenko and Y. G. Gogotsi, *Oxid. Met.*, **27**, 83–93 (1987).
27) S. Wu, H. M. Chan and M. P. Harmer, *J. Am. Cer. Soc.*, **80**, 1579–1582 (1997).
28) R. F. Davis and J. A. Pask, *J. Am. Ceram. Soc.*, **55**, 525–531 (1972).
29) P. Mechnich, H. Scheider, M. Schmucker and B. Saruhan, *J. Am. Ceram. Soc.*, **81**, 1931–1937 (1998).
30) V. A. Lavrenko and A. F. Alexeev, *Ceram. Int.*, **9**, 80–82 (1983).
31) Y.-H. Koh, J.-J. Choi and H.-E. Kim, *J. Am. Ceram. Soc.*, **83**, 306–310 (2000).